Chlorination of Hydrogenated Silicon Nanosheets Revealed by Solid-State Nuclear Magnetic Resonance Spectroscopy

Rick W. Dorn,[1,2] Bradley J. Ryan,[3] Sujeewa N. S. Lamahewage,[1,2] Mark V. Dodson,[1] Jeremy B. Essner,[3] Rana Biswas,[1,4] Matthew G. Panthani,[3*] Aaron J. Rossini[1,2*]

[1] US Department of Energy, Ames National Laboratory, Ames, IA, USA, 50011. [2] Iowa State University, Department of Chemistry, Ames, IA, USA, 50011. [3] Iowa State University, Department of Chemical and Biological Engineering, Ames, IA, USA 50011. [4] Iowa State University, Departments of Physics and Astronomy; Electrical and Computer Engineering and Microelectronics Research Center, Ames, IA, USA, 50011.

Supporting Information Placeholder

ABSTRACT: Two-dimensional silicon nanosheets (Si-NS) synthesized by topotactic deintercalation of $CaSi_2$ are hypothesized to consist of buckled layers of sp^3 hybridized silicon atoms that are bonded to three other framework Si atoms and a terminal atom or functional group such as H, Cl or a hydroxyl. Here, we apply $^1H\{^{35}Cl\}$ and $^{29}Si\{^{35}Cl\}$ Resonance-Echo Saturation-Pulse DOuble-Resonance (RESPDOR) solid-state NMR experiments to directly confirm the presence of chlorinated Si atoms within Si-NS. Plotting the $^1H\{^{35}Cl\}$ RESPDOR dephasing as a function of the ^{35}Cl saturation pulse offset reveals the ^{35}Cl quadrupolar coupling constant (C_Q) is 38 MHz, consistent with Cl atoms that are covalently bound to silicon. Modelling the $^1H\{^{35}Cl\}$ RESPDOR dephasing curve shows that the Si-Si interlayer spacing is approximately 6 Å. Plane-wave DFT calculations imply that the direct band gap transition of the Si-NS decreases with increasing chlorination, suggesting that chlorination can be used to tune the band gap.

Introduction

Two-dimensional silicon nanosheets (Si-NS) have attracted considerable attention for their potential as next-generation semiconductors for many electronic, optoelectronic, spintronic, energy storage and catalytic applications.[1-13] One route to making Si-NS is to perform topotactic deintercalation of alkali metal silicides, such as calcium disilicide ($CaSi_2$). $CaSi_2$ is de-intercalated by reacting it with aqueous HCl solution at *ca.* –30 °C. The resultant Si-NS are thought to adopt a buckled layered structure where each Si atom is bonded to three other framework Si atoms and a terminal atom/functional group (**Si**Si_3X, Figure 1A). We previously used 1D and 2D ^1H and ^{29}Si solid-state NMR experiments to show that the majority of the Si atoms are terminated with H atoms (**Si**Si_3H), leading to the conclusion that the structure of Si-NS can be best described as "silicane".[11] However, ^{29}Si solid-state NMR spectra reveal additional NMR signals hypothesized to arise from OH and Cl terminated Si atoms (**Si**Si_3OH and **Si**Si_3Cl, Figure 1A). Energy-dispersive X-ray spectroscopy (EDS) images, infrared spectroscopy (IR), and X-ray photoelectron spectroscopy (XPS) also suggest the presence of Cl terminated silicon atoms in Si-NS.[11]

The hypothesis that Si-NS are partially chlorinated is intriguing because halogenated Si-NS have been computationally predicted to exhibit smaller electronic band gaps as compared to fully hydrogenated Si-NS

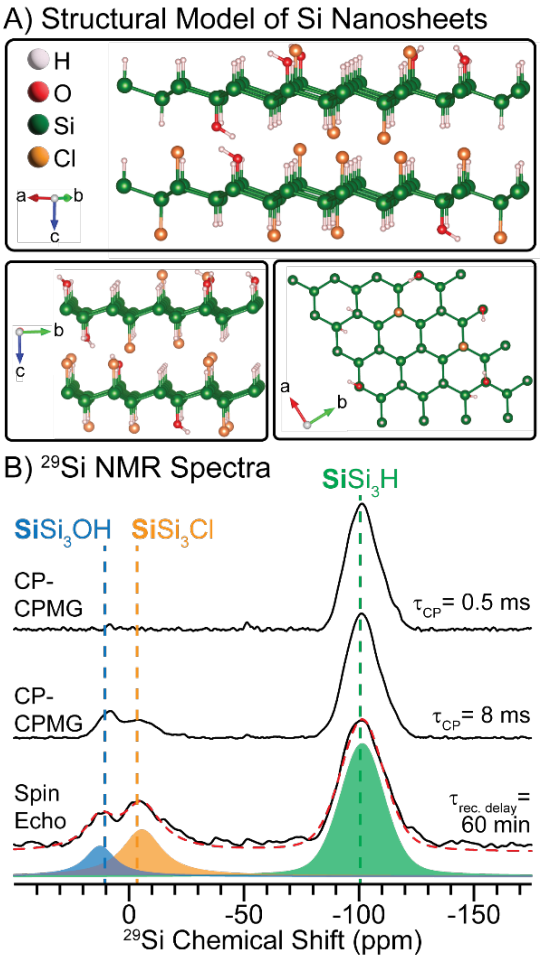

Figure 1. (A) Representative structural model of Si-NS containing **Si**Si_3H, **Si**Si_3OH and **Si**Si_3Cl groups. Note, this structure was not obtained with quantum chemical calculations. (B) 1D (upper, middle) $^1H \rightarrow {}^{29}Si$ CP-CPMG and (lower) direct excitation ^{29}Si NMR spectra of Si-NS. The dashed, red line corresponds to an analytical fit.

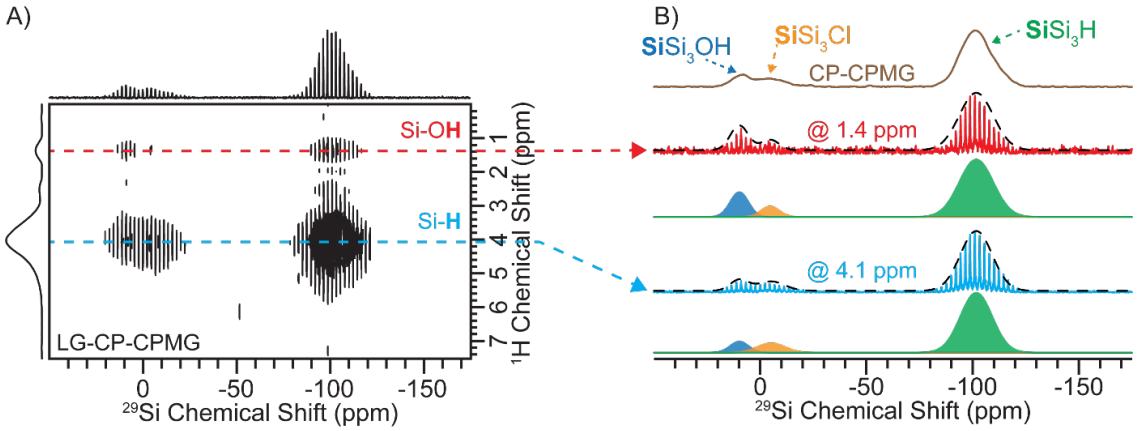

Figure 2. (A) 2D ^{1}H→^{29}Si (A) LG-CP HETCOR NMR spectrum of Si-NS recorded with an 8.928 kHz MAS frequency, CPMG during ^{29}Si acquisition and ^{1}H eDUMBO$_{1-22}$ homonuclear dipolar decoupling during ^{1}H chemical shift evolution. (B) ^{29}Si NMR spectra extracted from the indicated rows of the 2D HETCOR spectrum at ^{1}H shifts of (red) 1.4 or (blue) 4.1 ppm. The black dashed lines correspond to analytical simulations and the individual fitted peaks are shown below each row. A 1D ^{1}H→^{29}Si CP-CPMG spectrum recorded with a 7 ms contact time is shown for comparison (brown trace).

(silicane).[14-21] For example, chlorination or fluorination of Si-NS were predicted to decrease the electronic band gap by 0.78 or 1.29 eV, respectively.[15] Interestingly, prior density-functional theory (DFT) calculations suggested that the band gap could be tuned between 2.2 and 0.62 eV by controlling the extent of fluorination of polysilane.[14] Similar trends in band gap tunability were predicted for chlorinated germanane,[22] the germanium based analog of silicane.[23] Therefore, the identification of Cl terminated Si sites in Si-NS is highly important for understanding its electronic structure and optoelectronic properties.

It is generally challenging to probe the molecule structure of chlorinated sites in inorganic materials. Energy-filtered microscopy and XPS are commonly used to reveal Cl atoms but provide limited information about the chemical structure. ^{35}Cl has a nuclear spin of 3/2, a natural isotopic abundance of 75% and a gyromagnetic ratio close to that of ^{15}N, making it appealing for solid-state NMR experiments. However, acquisition of ^{35}Cl solid-state NMR spectra is often challenging because quadrupolar signal broadening results in central-transition (CT) NMR spectra that are typically megahertz broad, especially for terminal, covalently bonded Cl atoms.[24-37] ^{35}Cl solid-state NMR spectra are generally obtained under static conditions with Car-Purcell-Meiboom-Gill (CPMG) and frequency-stepped acquisition techniques.[24-37] Unfortunately, static ^{35}Cl solid-state NMR experiments often suffer from poor sensitivity and resolution. Here, we show that ^{1}H{^{35}Cl} and ^{29}Si{^{35}Cl} Resonance-Echo Saturation-Pulse DOuble-Resonance (RESPDOR) NMR experiments can be used to directly confirm the presence of chlorinated Si atoms in Si-NS. This approach should be generally applicable to rapidly detect the presence of Cl substituents in inorganic materials at routinely accessible magnetic fields.

Results and Discussion

Si-NS were synthesized via the topotactic deintercalation of $CaSi_2$ in aqueous HCl at *ca.* –30 °C; $CaSi_2$ was prepared via the melting of elemental Ca and Si.[11, 12] Note that the $CaSi_2$ used here was of very high purity and did not contain iron or bulk silicon impurities typically found in commercial $CaSi_2$.[11, 12] SEM EDS analysis indicates that the material studied here has a Si:Cl atomic ratio between 5.7 to 6.3 (Figures S1 and S2, Table S1, see *Supporting Information* for more discussion). Consistent with these results, our prior SEM EDS analysis of a different sample of Si-NS gave Si:Cl atomic ratios between 8 to 5.3, depending upon the portion of the sample that was imaged.[11] Yamanaka et al. used gravimetric analysis and measured an Si:Cl atomic ratio of 5.2 for Si-NS synthesized under similar conditions as the materials studied here.[13] We note that Yamanaka et al. attributed the presence Cl to HCl gas which was intercalated in between the silicon layers. However, as is shown below, NMR conclusively proves that Cl is covalently bonded to the Si atoms of the Si-NS.

Magic angle spinning (MAS) ^{29}Si solid-state NMR spectra of Si-NS were recorded with either direct excitation or ^{1}H→^{29}Si cross-polarization (CP) and CPMG for detection (Figure 1B). The ^{1}H→^{29}Si CP-CPMG NMR spectrum recorded with a long CP contact time (τ_{CP} = 8 ms) reveals three broad ^{29}Si NMR signals centered at *ca.* 10, –5 and –100 ppm. Only the ^{29}Si NMR signal at –100 ppm was observed with the use of a short CP contact time (τ_{CP} = 0.5 ms), confirming the assignment of the –100 ppm NMR signal to H terminated Si atoms (**Si**Si$_3$H).[11] We have also previously used ^{1}H→^{29}Si scalar-based (refocused INEPT) NMR experiments to confirm the assignment of **Si**Si$_3$H NMR signals.[11] As discussed below, the ^{29}Si NMR signals at *ca.* 10 and –5 ppm correspond to Si atoms terminated with an OH group (**Si**Si$_3$OH) or Cl atom (**Si**Si$_3$Cl), respectively. We previously used ^{29}Si homonuclear correlation NMR experiments to demonstrate that the **Si**Si$_3$OH and **Si**Si$_3$Cl NMR signals arise from silicon atoms that are covalently bonded to **Si**Si$_3$H units.[11] A quantitative direct excitation ^{29}Si NMR spectrum reveals that *ca.* 70 % of the Si atoms are H terminated, while **Si**Si$_3$OH and **Si**Si$_3$Cl correspond to *ca.* 10 and 20 % of Si atoms, respectively (Figure 1B, Figure S3 and *Supporting Information* for more discussion). NMR indicates 20% of the Si atoms are Cl terminated, corresponding to an Si:Cl atomic ratio of 5. Thus, NMR and SEM EDS show reasonable agreement for the measured Cl content, with the minor discrepancies likely arising because the SEM EDS measurements are surface-weighted.

Previous plane-wave density functional theory (DFT) calculations[11] and the calculations shown here for chlorine and hydroxyl terminated Si-NS (*vide infra*) suggest the ^{29}Si NMR signals at 10 ppm and –5 ppm likely correspond to Si atoms terminated with OH groups and Cl atoms, respectively. To experimentally confirm the presence of **Si**Si$_3$OH, we recorded a 2D ^{1}H→^{29}Si Lee-Goldberg CP (LG-CP) heteronuclear correlation (HETCOR) NMR spectrum[38, 39] with ^{1}H eDUMBO$_{1-22}$ homonuclear decoupling[40] applied during ^{1}H chemical shift evolution (Figure 2A). LG-CP suppresses ^{1}H-^{1}H spin-diffusion during the CP step and

yields a spectrum primarily free of relayed correlations.[38, 39] The 2D $^{1}H \rightarrow ^{29}Si$ LG-CP HETCOR spectrum reveals two ^{1}H NMR signals at 1.4 and 4.1 ppm. The ^{1}H NMR signal at 4.1 ppm corresponds to the Si-**H** hydride atoms and correlates with all ^{29}Si NMR signals.[11] All ^{29}Si NMR signals are observed due to the use of a long CP contact time and because **Si**Si_3H groups are homogenously distributed throughout the material. The 1.4 ppm ^{1}H NMR signal also correlates with all ^{29}Si NMR signals, suggesting the **Si**Si_3H groups are also homogenously distributed across the sheets. However, the ^{29}Si NMR signal at 10 ppm exhibits increased relative signal intensity in the row taken at a ^{1}H chemical shift of 1.4 ppm, suggesting this ^{29}Si NMR signal corresponds to Si terminated with an OH group (Figure 2B). The ^{1}H shift of 1.4 ppm is also typical for non-hydrogen bonded silanols, further corroborating our assignment.[41-43] The assignment of 1.4 ppm ^{1}H NMR signals to hydroxyl groups is also consistent with the absence of the these ^{1}H NMR signals from previously acquired 2D $^{1}H\{^{29}Si\}$ INEPT correlation spectra;[11] a 2-bond ^{29}Si-^{1}H scalar coupling is likely too weak to generate observable correlations in an INEPT experiment. But, the close spatial proximity of the OH hydrogen atom and the silicon atom (ca. 2.1 Å) explain the correlations observed in the LG-CP HETCOR spectrum.

Next, we performed $^{29}Si\{^{35}Cl\}$ phase-modulated RESPDOR (PM-RESPDOR)[44-48] NMR experiments to probe Cl terminated Si atoms. In the $^{29}Si\{^{35}Cl\}$ RESPDOR experiments rotational echo double resonance (REDOR)[49] pulses were applied to the ^{29}Si spins to recouple dipolar interactions to ^{35}Cl spins. In a $^{29}Si\{^{35}Cl\}$ PM-RESPDOR experiment, the ^{29}Si NMR signal will decrease in intensity due to the application of a ^{35}Cl saturation pulse, provided the ^{29}Si spin is in close spatial proximity (dipolar coupled) to ^{35}Cl. The rate of signal dephasing is dependent on the inverse cube of the Si-Cl internuclear distance. The $^{29}Si\{^{35}Cl\}$ PM-RESPDOR dipolar dephasing curve shows that both ^{29}Si NMR signals at *ca.* –5 and –100 ppm exhibit significant signal dephasing, directly confirming that Cl is incorporated within the sheets (Figure S4). However, the rate of signal dephasing is much faster for the –5 ppm ^{29}Si NMR signal. Numerical simulation of the $^{29}Si\{^{35}Cl\}$ RESPDOR experiment suggests that the Si-Cl internuclear distance is 2.1 Å, confirming that the –5 ppm ^{29}Si NMR signal corresponds to Cl terminated Si atoms (**Si**Si_3Cl, Figure S4). We note that $^{29}Si\{^{35}Cl\}$ PM-RESPDOR dephasing curve contains a significant amount of error due to the low sensitivity of the experiment. The $^{29}Si\{^{35}Cl\}$ RESPDOR experiment is challenging because of (1) the low natural abundance of ^{29}Si (5 %), (2) the large ^{35}Cl quadrupolar coupling constant (C_Q) of *ca.* 38 MHz (see below), and (3) a low ^{35}Cl saturation pulse radio-frequency (RF) field of 16.5 kHz that was achievable with the 4.0 mm HXY probe used for experiments.

To alleviate the challenges associated with the $^{29}Si\{^{35}Cl\}$ PM-RESPDOR experiment, we turn to fast magic angle spinning (MAS) $^{1}H\{^{35}Cl\}$ NMR experiments. The indirect detection of ^{35}Cl through ^{1}H is beneficial because ^{1}H exhibits a significantly higher gyromagnetic ratio than ^{29}Si and ^{1}H is *ca.* 100 % abundant. In addition, the use of a fast MAS probe equipped with a 1.3 mm diameter RF coil and use of a double resonance probe configuration enables access to higher ^{35}Cl RF fields of ca. 85 kHz that can provide significant signal dephasing in RESPDOR experiments.

1D $^{1}H\{^{35}Cl\}$ double-echo (DE) RESPDOR[50] NMR spectra were recorded with or without a ^{35}Cl saturation pulse and a 50 kHz MAS frequency (Figures 3A and 3B). In the DE RESPDOR experiments supercycled $(S)R4^2_1$ symmetry-based recoupling[51] was applied to the ^{1}H spins. The application of ^{35}Cl saturation pulse (τ_{sat} = 80 µs, $\nu_1(^{35}Cl)$ = 85 kHz) at an offset of 0 MHz from the reference ^{35}Cl Larmor frequency caused significant ^{1}H signal dephasing, confirming the presence of Cl atoms in Si-NS. The ^{35}Cl-filtered ^{1}H NMR spectrum was acquired in *ca.* 10 min with only *ca.* 5 mg of sample, demonstrating that ^{1}H-detection enables the rapid detection of Cl within inorganic materials. This is not too surprising as all ^{1}H nuclei are effectively dipolar coupled to ^{35}Cl because **Si**Si_3Cl groups are homogenously distributed throughout the sample. The DFT optimized models of the 20% Cl terminated Si-NS (vide infra) suggest that the closest ^{1}H-^{35}Cl internuclear distances are approximately 2.7 Å (intersheet) and 3.4 Å (intrasheet), corresponding to ^{1}H-^{35}Cl dipolar coupling constants of 598 Hz and 300 Hz, respectively. Furthermore, each ^{1}H spin will be dipole coupled to several ^{35}Cl spins on average, which further accelerates dipolar dephasing as compared to isolated spin pairs.

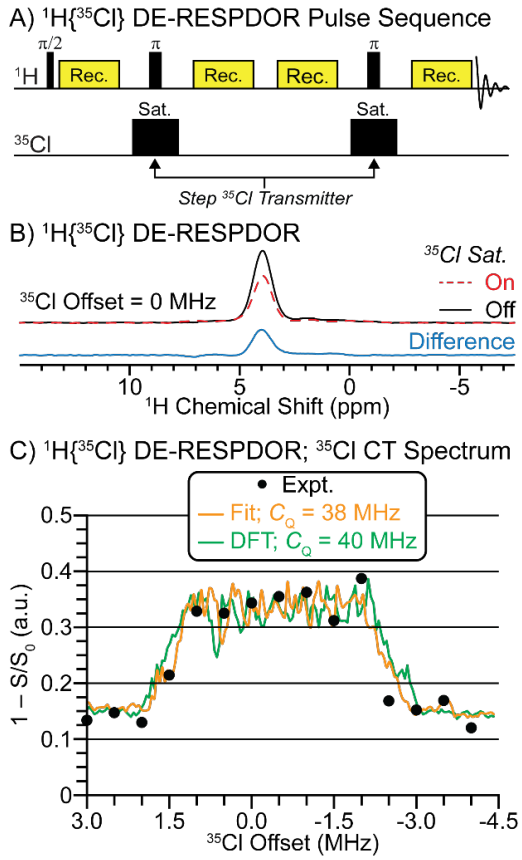

Figure 3. (A) $^{1}H\{^{35}Cl\}$ DE-RESPDOR pulse sequence. (B) 1D $^{1}H\{^{35}Cl\}$ DE-RESPDOR spectra recorded (red) with or (black) without a ^{35}Cl saturation pulse and $SR4^2_1$ dipolar recoupling applied for a total of 6.4 ms. The difference spectrum is shown below. (C) Plot of $^{1}H\{^{35}Cl\}$ DE-RESPDOR signal dephasing as a function of the ^{35}Cl transmitter offset. The circles and lines correspond to experimental data points and numerical SIMPSON simulations, respectively. Simulations are shown for the best fit ^{35}Cl C_Q of 38 MHz (orange) and a ^{35}Cl C_Q of 40 MHz (green) which was predicted by plane-wave DFT calculations. Experiments were performed with a B_0 of 14.1 T and a 50 kHz MAS frequency.

In order to fit the RESPDOR dephasing curves (Figure 4) and confirm that the Cl atoms are covalently bonded to Si the ^{35}Cl quadrupolar coupling constant (C_Q) must be measured. Plane-wave DFT calculations predict that the average ^{35}Cl C_Q is 40 MHz (standard deviation of 0.4 MHz), similar to the C_Q values of 38.4 MHz to 39.5 MHz previously measured with nuclear quadrupole resonance (NQR) spectroscopy for perchloropolysilanes.[52] Unfortunately, static ^{35}Cl WURST-CPMG experiments[24, 53, 54] on Si-NS did not yield any NMR signal after *ca.* 3 hours of acquisition (Figure S5). Based on the large predicted C_Q of 40 MHz

for Si-NS and the bandwidth of the WURST pulses, *ca.* 20-25 subspectra would be required to observe the entire quadrupolar powder pattern of Si-NS, making the static experiment impossible at a magnetic field of 14.1 T or less. In comparison, high signal-to-noise ^{35}Cl WURST-CPMG NMR signal was observed for transplatin in only *ca.* 8.5 minutes (Figure S5). Transplatin was used for comparison here because it has a Cl wt.% of 25 % and a ^{35}Cl C_Q of ca. 35 MHz, both of which are similar to Si-NS.[25] We note that we also attempted ^{35}Cl nuclear quadrupole resonance (NQR) experiments on the Si-NS to measure the ^{35}Cl C_Q, however, we could not observe any signal, like because of a distribution in C_Q which would broaden the NQR signals.

With the failure of the ^{35}Cl WURST-CPMG and NQR experiments on the Si-NS a different strategy was required to measure the ^{35}Cl NMR spectra and C_Q. Dipolar dephasing experiments have previously been used to indirectly detect wideline ^{14}N, ^{27}Al and ^{195}Pt NMR spectra via a spy nucleus such as ^{1}H or ^{13}C.[55-61] In these experiments, the spectrum of the indirectly detected nucleus is mapped out by plotting the observed dephasing as a function of the frequency offset of the saturation/inversion pulses that are applied to the indirectly detected spin. Recently, we described similar techniques to indirectly map out high-resolution, wideline MAS ^{195}Pt NMR spectra through a spy nucleus such as ^{1}H, ^{13}C or ^{31}P.[62,63] Motivated by these prior studies, we performed ^{1}H{^{35}Cl} DE-RESPDOR experiments on Si-NS where the offset of the ^{35}Cl saturation pulse offset was varied in steps of 500 kHz over a range of +3 to –4 MHz (Figure 3C). Plotting the signal dephasing as a function of the ^{35}Cl saturation pulse offset enables the reconstruction of the MAS ^{35}Cl central transition (CT) quadrupolar powder pattern for the Si-NS (Figure 3C). Notably, the ^{1}H-detected ^{35}Cl NMR spectrum of the Si-NS was acquired in only 1.4 hours at B_0 = 14.1 T. Numerical simulations of the ^{1}H{^{35}Cl} DE-RESPDOR dephasing profile suggest that the ^{35}Cl C_Q is *ca.* 38 MHz (with η = 0), in good agreement with the average ^{35}Cl C_Q value of 40 MHz predicted by plane-wave DFT calculations.

We also performed similar ^{1}H{^{35}Cl} DE-RESPDOR experiments on transplatin to confirm that this method provides accurate measurements of the ^{35}Cl C_Q. Excellent agreement was observed between the values of ^{35}Cl C_Q determined with DE-RESPDOR and WURST-CPMG (Figures S5 and S6).[25] The ^{35}Cl CT NMR spectrum of transplatin was acquired in just under 30 minutes with RESPDOR as compared to 3 hours for the static WURST-CPMG experiment. We note that in all ^{1}H{^{35}Cl} DE-RESPDOR experiments there is significant ^{1}H NMR signal dephasing even when the ^{35}Cl offset is off-resonance from the CT pattern. This dephasing arises due to saturation of the satellite transitions. To the best of our knowledge, this is the first demonstration of indirect detection of wideline spin I = 3/2 CT solid-state NMR spectra which are more than 1 MHz in breadth. Further investigation of the generality of RESPDOR experiments for indirect detection of I = 3/2 nuclei are underway.

With knowledge of the ^{35}Cl C_Q, the ^{1}H{^{35}Cl} DE-RESPDOR dephasing curve for the Si-NS can be modelled (Figure 4). To accurately simulate the dephasing curve, we built 20 Si-NS structural models, each consisting of two layers stacked on top of each other (Figure 4A). Within each model a Monte Carlo procedure was used to randomize the Cl positions based on the 20 % **Si**Si$_3$Cl population determined from direct excitation ^{29}Si NMR spectra and the ^{35}Cl natural abundance of 75 %.

In these models, we considered only the central H atom (colored red in Figure 4A) and calculated the internuclear distances between this H atom and all Cl atoms (Figure 4B). Multi-spin ^{1}H-^{35}Cl$_n$ (n = 1 – 3) numerical simulations were performed for all ^{1}H-^{35}Cl spin pairs within a 5 Å distance (Figure S7). Longer-range ^{1}H-^{35}Cl dipolar couplings were accounted for by running a two-spin ^{1}H-^{35}Cl numerical simulation that uses the calculated root sum square of the dipolar coupling constants for ^{1}H-^{35}Cl spin pairs with a distance > 5 Å and (see *Supporting Information* for more details about the fitting procedure). We then averaged the multi-spin numerical simulations over the ensemble of all 20 structures to obtain a curve that represents a random distribution of **Si**Si$_3$Cl species within Si-NS. Inclusion of long-range couplings is crucial to reproduce signal dephasing at recoupling durations longer than 3 ms (Figure S8). The shape of the dephasing curve is sensitive to the Si-Si interlayer spacing because interlayer distance is inversely correlated to inter-sheet ^{1}H-^{35}Cl dipolar couplings. Therefore, Si-Si interlayer spacings within the ensemble was set to 5 Å, 6 Å, or 7 Å. Comparison of the numerically simulated ^{1}H{^{35}Cl} DE-RESPDOR dephasing curves with the experimental dephasing curve reveals an interlayer spacing of *ca.* 6 Å gives best agreement with the experiments. This result is in excellent agreement with the spacing we determined in our previous synchrotron X-ray diffraction study.[12] Lastly, we used plane-wave DFT calculations to construct geometry optimized models of Si-NS containing 0, 20, 50 or 100 % Cl termination and a model with 20% Cl termination and 10% OH termination (Figure 5 and Figure S9). The calculations predict that the Si-Si interlayer distance increases with increasing chlorination to accommodate the longer Si-Cl bond length. The average interlayer spacing of 6.2 Å for

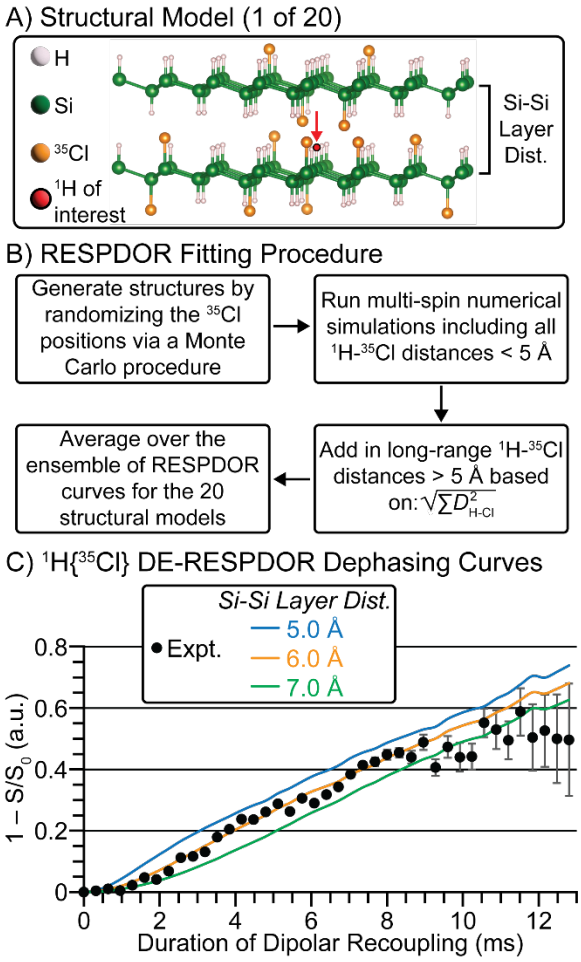

Figure 4. (A) 1 of 20 structural models of Si-NS with randomized positions of (orange) ^{35}Cl nuclei. The central, red H atom indicated by the arrow corresponds to the ^{1}H spin of interest. (B) General RESPDOR fitting procedure (see main-text and *Supporting Information*) for more details. (C) ^{1}H{^{35}Cl} DE-RESPDOR dephasing curves. The (black) circles correspond the experimental data points. The lines correspond to numerical simulations for Si-Si interlayer distances of (blue) 5, (orange) 6 or (green) 7 Å.

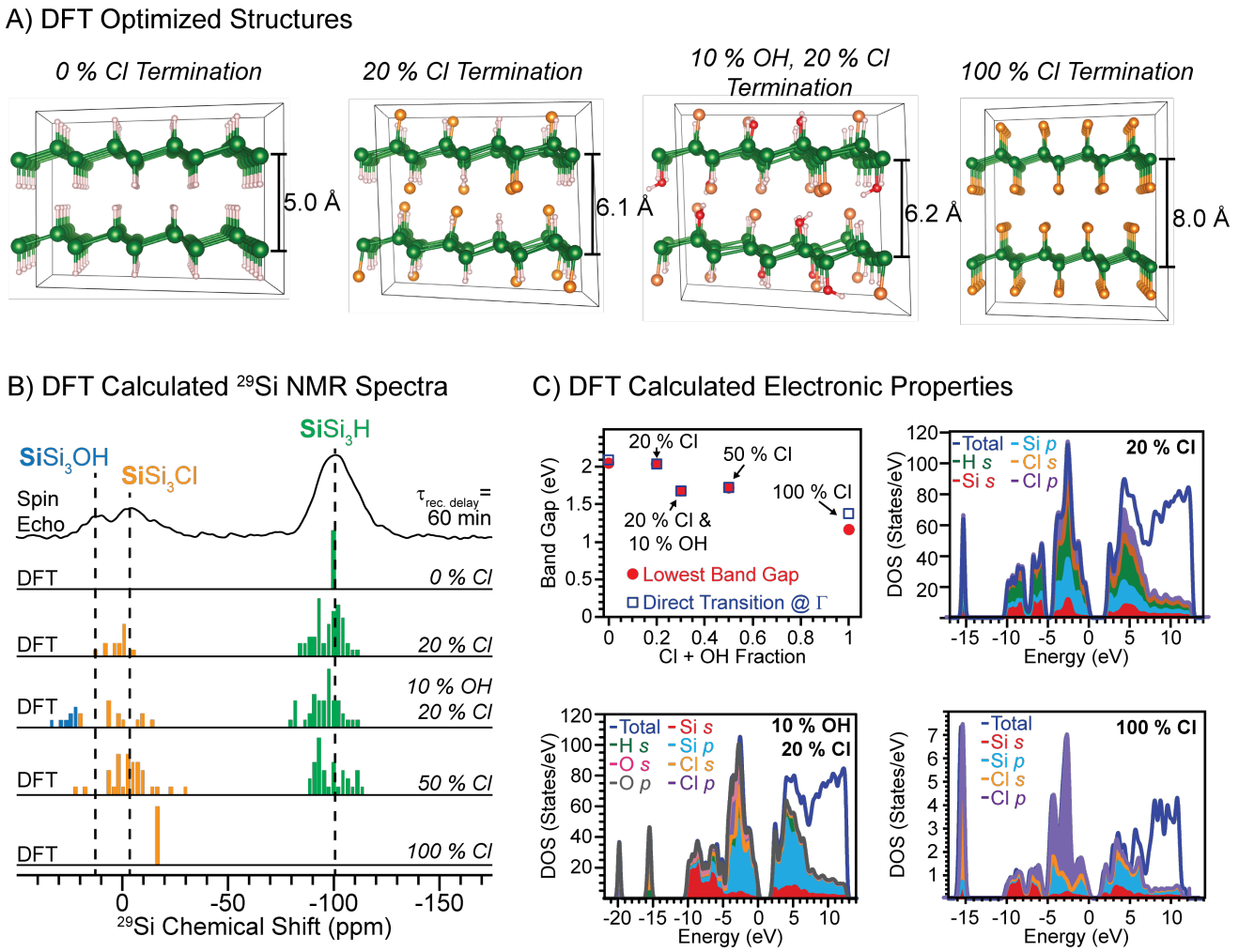

Figure 5. (A) DFT optimized structures of Si-NS containing 0, 20, or 100 % Cl termination and a model with 20% Cl and 10% OH termination. (B) Comparison of the (upper) experimental ^{29}Si NMR spectrum of Si-NS with (lower) ^{29}Si NMR spectra predicted by DFT plotted as histograms. (C) DFT calculated electronic band gaps and densities of states. Direct and indirect band gaps are indicated within the figure.

the 20 % Cl, 10% OH terminated model is in excellent agreement with the value of 6 Å determined from the ^{1}H{^{35}Cl} DE-RESPDOR dephasing curve. Interestingly, the models with partial chlorination or hydroxylation exhibit slightly distorted sheets as compared to the 0 or 100 % Cl terminated models (Figure 5A and Figure S9). GIPAW[64, 65] calculated chemical shifts predict large distribution in the ^{29}Si chemical shifts for models with intermediate chlorine content and partial hydroxylation, in good agreement with the experimental ^{29}Si NMR spectrum (Figure 5B).

We also calculated the electronic band structures and densities of states (DOS) for all Si-NS models (Figure 5C, see *Supporting Information* Figures S10 to S14 and additional discussions). Fully hydrogenated Si-NS (0 % Cl) exhibits a direct transition of 2.1 eV at the zone-center Γ and a slightly lower indirect band gap of 2.05 eV between A-Γ (Figure 5C and S10). 20 % chlorination slightly narrows the band gap (2.04 eV, (Figure 5C and S11). 50 % chlorination is predicted to significantly decrease the direct transition by *ca.* 0.32 eV (band gap = 1.73 eV; Figure 5C and S12). The model with 20% chlorination and 10% hydroxyl termination is predicted to have a direct band gap of 1.68 eV, which is below the predicted band gap of the 50% chlorinated structure. Fully chlorinated Si-NS exhibited the smallest band gap of 1.17 eV (Figure 5C and S10). The presence of a tunable direct transition via the chlorination and hydroxylation of Si-NS should provide new pathways for the synthesis of 2D silicon semiconductors for many material science applications. Experimentally, the controlled chlorination of Si-NS is likely feasible via the reaction of hydrogenated Si-NS with PCl_5 or Cl_2 as these reagents have been utilized for the chlorination of H-terminated Si(111) surfaces.[66-69] We hypothesize that controlled hydrolysis of chlorinated sites could then be used to modulate the hydroxyl group content. Further calculations should be performed to assess how varying the Cl and hydroxyl content could be used to tune the band structure.

Conclusions

^{1}H{^{35}Cl} and ^{29}Si{^{35}Cl} RESPDOR solid-state NMR experiments revealed chlorinated Si atoms in predominantly hydrogenated Si-NS. A quantitative ^{29}Si NMR spectrum showed that *ca.* 70 % of Si atoms are terminated with H atoms, while *ca.* 20 and 10 % of Si atoms are terminated by Cl and OH, respectively. The presence of hydroxyl groups was confirmed with ^{1}H-^{29}Si LG-CP HETCOR NMR experiments. Fast MAS ^{1}H{^{35}Cl} DE-RESPDOR experiments enabled the rapid detection of Cl within Si-NS. Importantly, we were able to indirectly observe the entire ^{35}Cl CT NMR spectrum by stepping the ^{35}Cl saturation pulse offset across the quadrupolar powder pattern in only *ca.* 1.4 hours at B_0 = 14.1 T. The determined ^{35}Cl C_Q of 38 MHz was in close agreement with that predicted by plane-wave DFT calculations (40 MHz). With knowledge

of the ^{35}Cl C_Q, the ^{1}H{^{35}Cl} RESPDOR dephasing curve could be modelled and revealed that the Si-Si interlayer spacing is *ca.* 6 Å. Lastly, plane-wave DFT predicted electronic band structures suggest that increasing chlorination leads to the emergence of a direct transition that decreases with increasing chlorination. The calculations also suggested that termination of silicon atoms with hydroxyl groups can also significantly reduce the band gap. The presence of a tunable direct band gap should enable the tailoring of 2D silicon semiconductors for many material science applications. ^{1}H{X} RESPDOR is a general method to rapidly map out CT quadrupolar powder patterns for $I = 3/2$ nuclei and that X{^{35}Cl} RESPDOR should be applicable to detect the presence of Cl substituents in many inorganic materials and catalysts. Our groups are exploring further research along these lines.

Experimental

Synthesis of Silicon Nanosheets (Si-Ns). Si-NS were synthesized via our previously reported procedure.[11, 12] In summary, $CaSi_2$ was prepared by melting Si and Ca (1:2 molar ratio of Ca to Si) in a sealed Ta tube inside an Ar-filled glovebox for *ca.* 1 minute. While the contents were still molten, the Ta tube was carefully inverted for a few minutes until the material started to solidify. This procedure of heating and cooling was repeated four times. On the final step, the Ta tube was cooled with Al chips and washed with first HCl and then DI water. The material was then dried and transferred back into the glovebox. The synthesized $CaSi_2$ was then ground in an N_2-filled glovebox. Approximately 3 g of the ground $CaSi_2$ was placed in a vial and cooled to −35 °C under N_2 overnight. Approximately 300 mL of concentrated aqueous HCl solution was added to a separate 500 mL round-bottom three-neck flask and cooled to −35 °C under N_2 overnight. The chilled $CaSi_2$ was added to the HCl solution the next day under a flow of N_2 and the reaction sat unstirred for 11 days. The contents of the reaction were filtered and washed with *ca.* 250 mL of anhydrous methanol and then *ca.* 50 mL of anhydrous acetonitrile under a flow of N_2. The Si-NS product was dried under vacuum for *ca.* 80 hours and stored inside a glovebox. Samples for solid-state NMR experiments were packed into the rotors inside of a glovebox.

Scanning electron microscopy (SEM) with energy dispersive X-ray spectroscopy (EDS). SEM-EDS was performed with a FEI Quanta 250 field-emission scanning electron microscope (FE-SEM) equipped with an Oxford Instruments X-Max 80 mm2 silicon drift detector. The Si-NS sample was prepared for characterization in a glovebox filled with N_2 by depositing the sample on a double coated, high purity conductive carbon Spectro tab (Ted Pella, Inc., #16084-4) affixed atop an aluminum SEM pin stub (Ted Pella, Inc., #16111). Specifically, a small quantity (approximately 5-10 mg) of the Si-NS sample was placed on a sheet of weighing paper and uniformly spread out across an area of 1.5 cm^2. The carbon tab covered pin stub was then carefully pressed against the sample until the desired level of sample coverage was achieved. The stub was transferred to a glass vial with an SEM pin mount gripper and was lightly tapped against the vial wall to knock off any loosely adhered sample. To minimize potential oxygen exposure during transportation to the characterization facility, the threads of the vial were wrapped with at least three full rotations of PTFE plumber's tape prior to caping while, after capping, three full rotations of electrical tape were wrapped around the cap/vial interface. The vial was kept in the glovebox until needed and in the N_2-filled vial until immediately before loading into the SEM. Prior to loading, the sample-coated stub was briefly blown off with compressed air to further remove any loosely adhered Si-NSs. During the loading and instrument preparation process, the Si-NS sample was exposed to air for no more than 10 min. The FE-SEM was operated at an electron accelerating voltage of 10 kV and the sample was characterized in low vacuum mode with a water vapor pressure of 40 Pa to minimize charging effects. For the EDS analyses, both targeted area spectra and elemental mapping were acquired with acquisition times of 30 sec and approximately 10 min, respectively. For the former, twenty different areas were assessed, including different stacks of nanosheets and multiple areas across an individual stack, while for the latter, elemental mapping was conducted on four distinct areas. All EDS data was initially processed with Oxford Instruments AZtec software prior to conducting statistical analyses and plotting.

Solid-State NMR Spectroscopy. Solid-state NMR spectroscopy experiments were performed on either a (^{1}H-^{29}Si and ^{29}Si-^{35}Cl experiments) 9.4 T Bruker wide-bore magnetic equipped with a Bruker AVANCE III HD console and either a Bruker (^{1}H-^{35}Cl of transplatin) 1.3 mm HX or (all other experiments) 4.0 mm HXY magic-angle spinning (MAS) NMR probe or a (^{1}H-^{35}Cl experiments) 14.1 T Bruker wide-bore magnet equipped with a Bruker AVANCE NEO console and a Phoenix 1.3 mm HXY MAS NMR probe. All experiments utilized N_2 gas for spinning. ^{1}H chemical shifts were referenced to 1 % tetramethylsilane (TMS) in $CDCl_3$ with adamantane (d_{iso}(^{1}H) = 1.71 ppm) as a secondary chemical shift reference. ^{29}Si chemical shifts were indirectly referenced to neat TMS using the IUPAC recommended relative NMR frequency.[70] NMR spectra were processed in Bruker Topspin (AVANCE III HD data) 3.6.1. or (AVANCE NEO data) 4.0.7. All experimental NMR parameters are given in Table S3.

The following experimental details are with respect to data acquired at B_0 = 9.4 T with the 4.0 mm HXY NMR probe (i.e., ^{1}H-^{29}Si, ^{29}Si-^{35}Cl, and static ^{35}Cl experiments). ^{1}H $\pi/2$ and π pulses were 2.5 and 5.0 μs in duration, respectively, corresponding to a 100 kHz radio frequency (RF) field. ^{29}Si $\pi/2$ and π pulses were either (^{1}H-^{29}Si experiments) 5 and 10 μs or (^{29}Si-^{35}Cl) 7 and 14 μs in duration, respectively, corresponding to 50 or 35.7 kHz RF field, respectively. The ^{35}Cl RF field was calibrated using the previous described heteronuclear Bloch-Siegert shift method with adamantane as the sample.[71] ^{1}H→^{29}Si cross-polarization (CP) was achieved with a 10 kHz MAS frequency with simultaneous ^{1}H and ^{29}Si spin-lock pulses with RF fields of *ca.* 42 (85-100 % RF field ramp, i.e., *ca.* 36-42 kHz RF field) and 24 kHz, respectively. ^{1}H→^{29}Si CP was achieved with an 8.928 kHz MAS frequency with simultaneous ^{1}H and ^{29}Si spin-lock pulses with RF fields of *ca.* 57 (85-100 % RF field ramp, i.e., *ca.* 49-57 kHz RF field) and 48 kHz, respectively. ^{1}H→^{29}Si Lee-Goldberg CP (LG-CP) was achieved with an 8.928 kHz MAS frequency with simultaneous ^{1}H and ^{29}Si spin-lock pulses with a *ca.* 44 and 43 (90-100 % RF field ramp, i.e., *ca.* 39-43 kHz) kHz RF field, respectively.[38] The ^{1}H transmitter offset was *ca.* 31 kHz, yielding an effective spin-lock RF field of *ca.* 53 kHz. The 2D ^{1}H→^{29}Si LG-CP HETCOR NMR spectrum was recorded with 100 kHz ^{1}H RF field of eDUMBO$_{1-22}$ homonuclear dipolar decoupling during the indirect dimension evolution of ^{1}H chemical shifts.[72] ^{29}Si{^{35}Cl} PM-RESPDOR experiments were performed with a 10 kHz MAS frequency and a 1 ms (i.e., 10 rotor cycle) ^{35}Cl PM saturation pulse with a *ca.* 16.5 kHz RF field.[45] The ^{29}Si{^{35}Cl} PM-RESPDOR experiments were recorded with a ^{35}Cl transmitter offset of *ca.* −1 MHz. Resonance-Echo DOuble-Resonance (REDOR) dipolar recoupling was applied to the ^{29}Si spins with a *ca.* 35.7 kHz RF field (14 μs π pulse) to re-introduce the ^{29}Si-^{35}Cl dipolar interaction under MAS. ^{1}H→^{29}Si CP was performed at the beginning of the experiment to increase overall sensitivity. All directly detected ^{29}Si NMR spectra (except for the ^{29}Si spin echo spectra) were recorded with Car-Purcell-Meiboom-Gill (CPMG) detection to increase sensitivity.[73] 100 kHz ^{1}H RF field SPINAL-64 heteronuclear decoupling was performed throughout the entire ^{29}Si{^{35}Cl} PM-RESPDOR experiment and during the acquisition of all ^{29}Si spectra.[74] Static ^{35}Cl WURST-CPMG experiments were performed with WURST pulses that were 50 μs in duration and with a sweep width of 800 kHz.[24, 53, 54] Each echo in the CPMG train was 90 μs in duration. A total of 100 echoes were acquired. 50 kHz ^{1}H RF field

SPINAL-64 decoupling was performed throughout the entire static experiments.[74] ^{1}H{^{35}Cl} DE-RESPDOR spectra of transplatin were recorded with the 1.3 mm HX NMR probe and a 50 kHz MAS frequency. The ^{1}H T_1 of transplatin was *ca.* 17 s; all experiments utilized a 5 s recycle delay. ^{1}H{^{35}Cl} DE-RESPDOR experiments were performed with ^{35}Cl saturation pulses that were 80 ms ($4 \times t_{rot}$) in duration with a 80 kHz RF field.[50] The $SR4_1^2$ heteronuclear dipolar recoupling sequence was applied to the ^{1}H spins to re-introduce the ^{1}H-^{35}Cl dipolar interaction under MAS.[51] A control (without a ^{35}Cl saturation pulse) and dephased (with a ^{35}Cl saturation pulse) point was recorded at each ^{35}Cl offset.

The following experimental details are with respect to data acquired at B_0 = 14.1 T (i.e., ^{1}H-^{35}Cl experiments). All ^{1}H-^{35}Cl NMR experiments were performed a Phoenix HXY probe equipped with a 1.3 mm stator. The MAS frequency was 50 kHz for all experiments. ^{1}H $\pi/2$ and π pulses were 2.5 and 5.0 μs in duration, respectively, corresponding to a 100 kHz RF field. The ^{35}Cl RF field was calibrated using the previous described heteronuclear Bloch-Siegert shift method with adamantane as the sample.[71] ^{1}H{^{35}Cl} DE-RESPDOR experiments were performed with ^{35}Cl saturation pulses that were either (dipolar dephasing curve) 30 μs ($1.5 \times \tau_{rot}$) or 80 μs ($4 \times t_{rot}$) in duration and with RF fields of *ca.* 89 or 85 kHz, respectively.[50] The 80 μs saturation pulse was used for mapping of the ^{35}Cl CT quadrupolar powder pattern. The $SR4_1^2$ heteronuclear dipolar recoupling sequence was applied to the ^{1}H spins to re-introduce the ^{1}H-^{35}Cl dipolar interaction under MAS.[51] The ^{1}H{^{35}Cl} DE-RESPDOR dipolar dephasing curve of Si-NS was recorded with a ^{35}Cl transmitter offset of *ca.* –657 kHz. The ^{35}Cl channel of the NMR probe was re-tuned for each ^{35}Cl transmitter offset used to indirectly map out the ^{35}Cl CT quadrupolar powder pattern. Only one control point (i.e., no ^{35}Cl saturation pulse) was recorded while dephasing points (i.e., with a ^{35}Cl saturation pulse) were recorded at all ^{35}Cl transmitter offsets.

Numerical Solid-State NMR Spectroscopy Simulations. Numerical solid-state NMR simulations were performed using SIMPSON v4.2.1.[75-77] All numerical simulations were performed with parameters (i.e., RF fields, transmitter offsets and B_0) identical to those used experimentally. ^{29}Si{^{35}Cl} PM-RESPDOR numerical simulations were performed with a two spin ^{29}Si-^{35}Cl spin system, the rep168 crystal file, 10 γ angles and a 1 μs maximum time duration where the Hamiltonian was considered time independent. Numerical simulations of the ^{1}H{^{35}Cl} DE-RESPDOR dipolar dephasing curve were performed with either two, three or four ^{1}H-^{35}Cl$_n$ (n = 1, 2 or 3) spin systems, the rep168 crystal file, and 8 γ angles. ^{1}H-^{35}Cl dipolar β Euler angles were either 30, 45 or 90° for ^{35}Cl that was *trans* (intra-sheet, opposite side), inter-sheet, or *cis* (intra-sheet, same side) to ^{1}H, respectively. Numerical simulations of the ^{1}H{^{35}Cl} DE-RESPDOR experiment used to map out the ^{35}Cl CT quadrupolar powder pattern of Si-NS and transplatin were performed with a two spin ^{1}H-^{35}Cl spin system, the zcw4180 crystal file, and 13 γ angles. The ^{35}Cl transmitter frequency was incremented in steps of 47.5 kHz or 50 kHz for Si-NS or transplatin, respectively.

Plane-wave Density Functional Theory Calculations. Plane-wave density functional theory (DFT) calculations were performed in CASTEP version 2017 T2[78] utilizing the gauge-including projector-augmented eave (GIPAW) approach.[64] The atomic coordinates and unit cell parameters of the Si-NS models were geometry optimized using the BFGS geometry optimization method[79] and converged to a maximum displacement threshold of 5.0×10^{-4} Å, an energy threshold of 5.0×10^{-6} eV/atom, a maximum force threshold of 0.01 eV/Å and a maximum stress threshold of 0.02 GPa. Geometry optimization and GIPAW NMR calculations utilized the Generalized Gradient Approximation (GGA) with the Perdew-Burke Ernzerhof (PBE) exchange-correlation functional,[79] Tkatchenko-Scheffler dispersion corrections,[80] On-the-Fly ultrasoft pseudopotentials (default settings as implemented in CASTEP version 2017 T2),[65, 81] zeroth-order regular approximation relativist treatments,[82] and a 630 eV kinetic energy cutoff. A 0.03 and 0.07 Å^{-1} k-point spacing was used for the NMR (with an energy calculation) and geometry optimization calculations, respectively. ^{29}Si isotropic shieldings (σ_{iso}) were converted to isotropic shifts (δ_{iso}) via a previously published calibration curve using identical calculation parameters.[11] The electronic band structures, total densities of state (DOS), projected DOS and optical absorptions were calculated on the geometry-optimized structures. The primitive cell was utilized for the 0 and 100 % Cl-terminated models. The full cell was utilized for the 20% and 50 % Cl-terminated models and 20% Cl- and 10%-OH terminated models. The primitive cell was used for the calculations of bulk crystalline Si. The DOS calculations used an energy smearing of 0.15 eV and 100 sampling points per eV. We note that the absolute values of the DFT calculated band gaps may be underestimated compared to experiment; however, the trends in the band gap are expected to be modelled well.

ASSOCIATED CONTENT

Supporting Information

The Supporting Information is available free of charge on the ACS Publications website and includes experimental details, additional NMR spectra, molecular coordinates from plane-wave DFT calculations and RESPDOR -derived structural models, and SIMPSON input files.

Raw NMR data is available for download at DO:10.5281/zenodo.7080307.

AUTHOR INFORMATION

Corresponding Author

Mathew G. Panthani – Email: panthani@iastate.edu
Aaron J. Rossini – Email: arossini@iastate.edu

Notes

The authors declare no competing financial interests.

ACKNOWLEDGMENT

This work was primarily supported by the US Department of Energy, Office of Science, Basic Energy Sciences, Materials Science and Engineering Division. Synthesis of Si-NS was supported by the Department of Defense (DoD) Air Force Office of Scientific Research (AFOSR) under award number FA9550-20-1-0018 and the National Science Foundation Early CAREER Development Award (DMR-1847370). M.V.D. is grateful to the U.S. Department of Energy Office of Science Undergraduate Laboratory Internship (SULI) program for assistantship and the opportunity to participate in the SULI program. The Ames National Laboratory is operated for the US Department of Energy by Iowa State University under contract DE-AC02-07CH11358. A.J.R. acknowledges additional support from the Alfred P. Sloan Foundation through a Sloan research fellowship.

REFERENCES

1. Liu, C.-C.; Feng, W.; Yao, Y., Quantum Spin Hall Effect in Silicene and Two-Dimensional Germanium. *Phys. Rev. Lett.* **2011,** 107, 076802.
2. Zhang, F.-B.; Lv, S.-F.; Jiang, J.-X.; Ni, Y., Preparation of siloxene nanosheet-supported palladium as sustainable catalyst for

Mizoroki–Heck reaction. *Appl. Organomet. Chem.* **2014,** 28, (11), 826-830.
3. Kumai, Y.; Nakano, H., Characteristics of layered polysilane and its application to lithium ion battery anodes. *Jpn. J. Appl. Phys.* **2015,** 54, 035201.
4. Tao, L.; Cinquanta, E.; Chiappe, D.; Grazianetti, C.; Fanciulli, M.; Dubey, M.; Molle, A.; Akinwande, D., Silicene field-effect transistors operating at room temperature. *Nat. Nanotechnol.* **2015,** 10, 227-231.
5. Imagawa, H.; Itahara, H., Stabilized lithium-ion battery anode performance by calcium-bridging of two dimensional siloxene layers. *Dalton Trans.* **2017,** 46, 3655-3660.
6. Liu, J.; Yang, Y.; Lyu, P.; Nachtigall, P.; Xu, Y., Few-Layer Silicene Nanosheets with Superior Lithium-Storage Properties. *Adv. Mater.* **2018,** 30, 1800838.
7. Krishnamoorthy, K.; Pazhamalai, P.; Kim, S.-J., Two-dimensional siloxene nanosheets: novel high-performance supercapacitor electrode materials. *Energy Environ. Sci.* **2018,** 11, 1595-1602.
8. Karar, D.; Bandyopadhyay, N. R.; Pramanick, A. K.; Acharyya, D.; Conibeer, G.; Banerjee, N.; Kusmartseva, O. E.; Ray, M., Quasi-Two-Dimensional Luminescent Silicon Nanosheets. *J. Phys. Chem. C* **2018,** 122, 18912-18921.
9. Qian, C.; Sun, W.; Hung, D. L. H.; Qiu, C.; Makaremi, M.; Hari Kumar, S. G.; Wan, L.; Ghoussoub, M.; Wood, T. E.; Xia, M.; Tountas, A. A.; Li, Y. F.; Wang, L.; Dong, Y.; Gourevich, I.; Singh, C. V.; Ozin, G. A., Catalytic CO2 reduction by palladium-decorated silicon–hydride nanosheets. *Nat. Catal.* **2019,** 2, 46-54.
10. Yan, X.; Sun, W.; Fan, L.; Duchesne, P. N.; Wang, W.; Kübel, C.; Wang, D.; Kumar, S. G. H.; Li, Y. F.; Tavasoli, A.; Wood, T. E.; Hung, D. L. H.; Wan, L.; Wang, L.; Song, R.; Guo, J.; Gourevich, I.; Jelle, A. A.; Lu, J.; Li, R.; Hatton, B. D.; Ozin, G. A., Nickel@Siloxene catalytic nanosheets for high-performance CO2 methanation. *Nat. Commun.* **2019,** 10, 2608.
11. Ryan, B. J.; Hanrahan, M. P.; Wang, Y.; Ramesh, U.; Nyamekye, C. K. A.; Nelson, R. D.; Liu, Z.; Huang, C.; Whitehead, B.; Wang, J.; Roling, L. T.; Smith, E. A.; Rossini, A. J.; Panthani, M. G., Silicene, Siloxene, or Silicane? Revealing the Structure and Optical Properties of Silicon Nanosheets Derived from Calcium Disilicide. *Chem. Mater.* **2020,** 32, 795-804.
12. Ryan, B. J.; Roling, L. T.; Panthani, M. G., Anisotropic Disorder and Thermal Stability of Silicane. *ACS Nano* **2021,** 15, 14557-14569.
13. Yamanaka, S.; Matsu-ura, H.; Ishikawa, M., New deintercalation reaction of calcium from calcium disilicide. Synthesis of layered polysilane. *Mater. Res. Bull.* **1996,** 31, 307-316.
14. Lu, N.; Li, Z.; Yang, J., Electronic Structure Engineering via On-Plane Chemical Functionalization: A Comparison Study on Two-Dimensional Polysilane and Graphane. *J. Phys. Chem. C.* **2009,** 113, 16741-16746.
15. Gao, N.; Zheng, W. T.; Jiang, Q., Density functional theory calculations for two-dimensional silicene with halogen functionalization. *Phys. Chem. Chem. Phys.* **2012,** 14, 257-261.
16. Ding, Y.; Wang, Y., Electronic structures of silicene fluoride and hydride. *Appl. Phys. Lett.* **2012,** 100, 083102.
17. Gao, N.; Li, J. C.; Jiang, Q., Bandgap opening in silicene: Effect of substrates. *Chem. Phys. Lett.* **2014,** 592, 222-226.
18. Zhang, W.-B.; Song, Z.-B.; Dou, L.-M., The tunable electronic structure and mechanical properties of halogenated silicene: a first-principles study. *J. Mater. Chem. C* **2015,** 3, 3087-3094.
19. Sun, M.; Ren, Q.; Wang, S.; Yu, J.; Tang, W., Electronic properties of Janus silicene: new direct band gap semiconductors. *J. Phys. D: Appl. Phys.* **2016,** 49, 445305.
20. Zaminpayma, E.; Nayebi, P., Band gap engineering in silicene: A theoretical study of density functional tight-binding theory. *Physica E Low Dimens. Syst. Nanostruct.* **2016,** 84, 555-563.
21. Tang, W.; Sun, M.; Ren, Q.; Zhang, Y.; Wang, S.; Yu, J., First principles study of silicene symmetrically and asymmetrically functionalized with halogen atoms. *RSC Advances* **2016,** 6, 95846-95854.
22. Xiao, P.; Fan, X.-L.; Liu, L.-M., Tuning the electronic properties of half- and full-hydrogenated germanene by chlorination and hydroxylation: A first-principles study. *Comput. Mater. Sci.* **2014,** 92, 244-252.
23. Bianco, E.; Butler, S.; Jiang, S.; Restrepo, O. D.; Windl, W.; Goldberger, J. E., Stability and Exfoliation of Germanane: A Germanium Graphane Analogue. *ACS Nano* **2013,** 7, (5), 4414-4421.
24. Rossini, A. J.; Mills, R. W.; Briscoe, G. A.; Norton, E. L.; Geier, S. J.; Hung, I.; Zheng, S.; Autschbach, J.; Schurko, R. W., Solid-State Chlorine NMR of Group IV Transition Metal Organometallic Complexes. *J. Am. Chem. Soc.* **2009,** 131, 3317-3330.
25. Lucier, B. E. G.; Reidel, A. R.; Schurko, R. W., Multinuclear solid-state NMR of square-planar platinum complexes — Cisplatin and related systems. *Can. J. Chem.* **2011,** 89, 919-937.
26. Perras, F. A.; Bryce, D. L., Direct Investigation of Covalently Bound Chlorine in Organic Compounds by Solid-State ^{35}Cl NMR Spectroscopy and Exact Spectral Line-Shape Simulations. *Angew. Chem. Int. Ed.* **2012,** 51, 4227-4230.
27. Johnston, K. E.; O'Keefe, C. A.; Gauvin, R. M.; Trébosc, J.; Delevoye, L.; Amoureux, J.-P.; Popoff, N.; Taoufik, M.; Oudatchin, K.; Schurko, R. W., A Study of Transition-Metal Organometallic Complexes Combining ^{35}Cl Solid-State NMR Spectroscopy and ^{35}Cl NQR Spectroscopy and First-Principles DFT Calculations. *Chem. Eur. J.* **2013,** 19, 12396-12414.
28. Schurko, R. W., Ultra-Wideline Solid-State NMR Spectroscopy. *Acc. Chem. Res.* **2013,** 46, 1985-1995.
29. O'Keefe, C. A.; Johnston, K. E.; Sutter, K.; Autschbach, J.; Gauvin, R.; Trébosc, J.; Delevoye, L.; Popoff, N.; Taoufik, M.; Oudatchin, K.; Schurko, R. W., An Investigation of Chlorine Ligands in Transition-Metal Complexes via ^{35}Cl Solid-State NMR and Density Functional Theory Calculations. *Inorg. Chem.* **2014,** 53, (18), 9581-9597.
30. Hanson, M. A.; Terskikh, V. V.; Baines, K. M.; Huang, Y., Chlorine-35 Solid-State NMR Spectroscopy as an Indirect Probe of Germanium Oxidation State and Coordination Environment in Germanium Chlorides. *Inorg. Chem.* **2014,** 53, 7377-7388.
31. Viger-Gravel, J.; Leclerc, S.; Korobkov, I.; Bryce, D. L., Direct Investigation of Halogen Bonds by Solid-State Multinuclear Magnetic Resonance Spectroscopy and Molecular Orbital Analysis. *J. Am. Chem. Soc.* **2014,** 136, 6929-6942.
32. Lucier, B. E. G.; Johnston, K. E.; Xu, W.; Hanson, J. C.; Senanayake, S. D.; Yao, S.; Bourassa, M. W.; Srebro, M.; Autschbach, J.; Schurko, R. W., Unravelling the Structure of Magnus' Pink Salt. *J. Am. Chem. Soc.* **2014,** 136, 1333-1351.
33. Terskikh, V. V.; Pawsey, S.; Ripmeester, J. A., High-field solid-state ^{35}Cl NMR in selenium(IV) and tellurium(IV) hexachlorides. *Journal of Structural Chemistry* **2016,** 57, 308-318.
34. Szell, P. M. J.; Bryce, D. L., Chapter Three - Recent advances in chlorine, bromine, and iodine solid-state NMR spectroscopy. In *Annual Reports on NMR Spectroscopy*, Webb, G. A., Ed. Academic Press: 2020; Vol. 100, pp 97-152.

35. Lucier, B. E. G.; Terskikh, V. V.; Guo, J.; Bourque, J. L.; McOnie, S. L.; Ripmeester, J. A.; Huang, Y.; Baines, K. M., Chlorine-35 Solid-State Nuclear Magnetic Resonance Spectroscopy as an Indirect Probe of the Oxidation Number of Tin in Tin Chlorides. *Inorg. Chem.* **2020,** 59, 13651-13670.
36. Piveteau, L.; Aebli, M.; Yazdani, N.; Millen, M.; Korosec, L.; Krieg, F.; Benin, B. M.; Morad, V.; Piveteau, C.; Shiroka, T.; Comas-Vives, A.; Copéret, C.; Lindenberg, A. M.; Wood, V.; Verel, R.; Kovalenko, M. V., Bulk and Nanocrystalline Cesium Lead-Halide Perovskites as Seen by Halide Magnetic Resonance. *ACS Cent. Sci.* **2020,** 6, 1138-1149.
37. Sarkar, D.; Hooper, R. W.; Karmakar, A.; Bhattacharya, A.; Pominov, A.; Terskikh, V. V.; Michaelis, V. K., Metal Halide Perovskite and Perovskite-like Materials through the Lens of Ultra-wideline $^{35/37}$Cl NMR Spectroscopy. *ACS Mater. Lett.* **2022,** 4, 1255-1263.
38. Ladizhansky, V.; Vega, S., Polarization transfer dynamics in Lee–Goldburg cross polarization nuclear magnetic resonance experiments on rotating solids. *J. Chem. Phys.* **2000,** 112, 7158-7168.
39. van Rossum, B. J.; de Groot, C. P.; Ladizhansky, V.; Vega, S.; de Groot, H. J. M., A Method for Measuring Heteronuclear (1H–13C) Distances in High Speed MAS NMR. *J. Am. Chem. Soc.* **2000,** 122, 3465-3472.
40. Elena, B.; de Paepe, G.; Emsley, L., Direct spectral optimisation of proton-proton homonuclear dipolar decoupling in solid-state NMR. *Chem. Phys. Lett.* **2004,** 398, 532-538.
41. Hwang, S.-J.; Chen, C.-Y.; Zones, S. I., Boron Sites in Borosilicate Zeolites at Various Stages of Hydration Studied by Solid State NMR Spectroscopy. *J. Phys. Chem. B* **2004,** 108, 18535-18546.
42. Trébosc, J.; Wiench, J. W.; Huh, S.; Lin, V. S. Y.; Pruski, M., Solid-State NMR Study of MCM-41-type Mesoporous Silica Nanoparticles. *J. Am. Chem. Soc.* **2005,** 127, 3057-3068.
43. Cendejas, M. C.; Dorn, R. W.; McDermott, W. P.; Lebrón-Rodríguez, E. A.; Mark, L. O.; Rossini, A. J.; Hermans, I., Controlled Grafting Synthesis of Silica-Supported Boron for Oxidative Dehydrogenation Catalysis. *J. Phys. Chem. C* **2021,** 125, 12636-12649.
44. Chen, L.; Wang, Q.; Hu, B.; Lafon, O.; Trébosc, J.; Deng, F.; Amoureux, J.-P., Measurement of hetero-nuclear distances using a symmetry-based pulse sequence in solid-state NMR. *Phys. Chem. Chem. Phys.* **2010,** 12, 9395-9405.
45. Nimerovsky, E.; Gupta, R.; Yehl, J.; Li, M.; Polenova, T.; Goldbourt, A., Phase-modulated LA-REDOR: A robust, accurate and efficient solid-state NMR technique for distance measurements between a spin-1/2 and a quadrupole spin. *J. Magn. Reson.* **2014,** 244, 107-113.
46. Duong, N. T.; Rossi, F.; Makrinich, M.; Goldbourt, A.; Chierotti, M. R.; Gobetto, R.; Nishiyama, Y., Accurate 1H-14N Distance Measurements by Phase-Modulated RESPDOR at Ultra-Fast MAS. *J. Magn. Reson.* **2019,** 308, 106559.
47. Makrinich, M.; Sambol, M.; Goldbourt, A., Distance measurements between carbon and bromine using a split-pulse PM-RESPDOR solid-state NMR experiment. *Phys. Chem. Chem. Phys.* **2020,** 22, 21022-21030.
48. Gullion, T., Measurement of Dipolar Interactions Between Spin-1/2 and Qudarupolar Nuclei by Rotational-Echo, Adiabatic Passage, Double-Resonance NMR. *Chem. Phys. Lett.* **1995,** 246, 325-330.
49. Gullion, T.; Schaefer, J., Rotational-Echo Double-Resonance NMR. *J. Magn. Reson.* **1989,** 81, 196-200.
50. Atterberry, B. A.; Carnahan, S. L.; Chen, Y.; Venkatesh, A.; Rossini, A. J., Double echo symmetry-based REDOR and RESPDOR pulse sequences for proton detected measurements of heteronuclear dipolar coupling constants. *J. Magn. Reson.* **2022,** 336, 107147.
51. Brinkmann, A.; Kentgens, A. P. M., Proton-selective O-17-H-1 distance measurements in fast magic-angle-spinning solid-state NMR spectroscopy for the determination of hydrogen bond lengths. *J. Am. Chem. Soc.* **2006,** 128, 14758-14759.
52. Voronkov, M. G.; Feshin, V. P.; Nikitin, P. A.; Hengge, E.; Schmölzer, H., NQR 35Cl spectra of perchloropolysilanes. *J. Mol. Struct.* **1985,** 127, 181-183.
53. O'Dell, L. A.; Schurko, R. W., QCPMG using adiabatic pulses for faster acquisition of ultra-wideline NMR spectra. *Chem. Phys. Lett.* **2008,** 464, 97-102.
54. O'Dell, L. A.; Rossini, A. J.; Schurko, R. W., Acquisition of ultra-wideline NMR spectra from quadrupolar nuclei by frequency stepped WURST–QCPMG. *Chem. Phys. Lett.* **2009,** 468, 330-335.
55. Makowka, C. D.; Slichter, C. P.; Sinfelt, J. H., Probe of the Surface of a Heterogeneous Catalyst: Double NMR of Carbon Monoxide Chemisorbed on Highly Dispersed Platinum. *Phys. Rev. Lett.* **1982,** 49, (6), 379-382.
56. Makowka, C. D.; Slichter, C. P.; Sinfelt, J. H., NMR of platinum catalysts: Double NMR of chemisorbed carbon monoxide and a model for the platinum NMR line shape. *Phys. Rev. B* **1985,** 31, (9), 5663-5679.
57. Grey, C. P.; Vega, A. J., Determination of the Quadrupole Coupling Constant of the Invisible Aluminum Spins in Zeolite HY with 1H/27Al TRAPDOR NMR. *J. Am. Chem. Soc.* **1995,** 117, 8232-8242.
58. Grey, C. P.; Veeman, W. S., The Detection of Weak Heteronuclear Coupling Between Spin 1 and Spin 1/2 Nuclei in MAS NMR; ^{14}N/^{13}C/^{1}H Triple Resonance Experiments. *Chem. Phys. Lett.* **1992,** 192, 379-385.
59. Kalwei, M.; Koller, H., Quantitative Comparison of REAPDOR and TRAPDOR Experiments by Numerical Simulations and Determination of H–Al Distances in Zeolites. *Solid State Nucl. Magn. Reson.* **2002,** 21, 145-157.
60. Gan, Z., Measuring nitrogen quadrupolar coupling with ^{13}C detected wide-line ^{14}N NMR under magic-angle spinning. *Chem. Commun.* **2008**, 868-870.
61. Jaroszewicz, M. J.; Altenhof, A. R.; Schurko, R. W.; Frydman, L., Sensitivity Enhancement by Progressive Saturation of the Proton Reservoir: A Solid-State NMR Analogue of Chemical Exchange Saturation Transfer. *J. Am. Chem. Soc.* **2021,** 143, 19778-19784.
62. Venkatesh, A.; Gioffrè, D.; Atterberry, B. A.; Rochlitz, L.; Carnahan, S. L.; Wang, Z.; Menzildjian, G.; Lesage, A.; Copéret, C.; Rossini, A. J., Molecular and Electronic Structure of Isolated Platinum Sites Enabled by the Expedient Measurement of ^{195}Pt Chemical Shift Anisotropy. *J. Am. Chem. Soc.* **2022**, 144, 13511-13525.
63. Wang, Z.; Völker, L. A.; Robinson, T. C.; Kaeffer, N.; Menzildjian, G.; Jabbour, R.; Venkatesh, A.; Gajan, D.; Rossini, A. J.; Copéret, C.; Lesage, A., Speciation and Structures in Pt Surface Sites Stabilized by N-Heterocyclic Carbene Ligands Revealed by Dynamic Nuclear Polarization Enhanced Indirectly Detected 195Pt NMR Spectroscopic Signatures and Fingerprint Analysis. *J. Am. Chem. Soc.*, **2022**, 144, DOI:10.1021/jacs.2c08300.
64. Pickard, C. J.; Mauri, F., All-Electron Magnetic Response with Pseudopotentials: NMR Chemical Shifts. *Phys. Rev. B* **2001,** 63, 245101.
65. Yates, J. R.; Pickard, C. J.; Mauri, F., Calculation of NMR Chemical Shifts for Extended Systems using Ultrasoft Pseudopotentials. *Phys. Rev. B* **2007,** 76, 024401.
66. Bansal, A.; Li, X.; Yi, S. I.; Weinberg, W. H.; Lewis, N. S., Spectroscopic Studies of the Modification of Crystalline Si(111) Surfaces with Covalently-Attached Alkyl Chains Using a

Chlorination/Alkylation Method. *J. Phys. Chem. B* **2001,** 105, 10266-10277.
67. Webb, L. J.; Lewis, N. S., Comparison of the Electrical Properties and Chemical Stability of Crystalline Silicon(111) Surfaces Alkylated Using Grignard Reagents or Olefins with Lewis Acid Catalysts. *J. Phys. Chem. B* **2003,** 107, 5404-5412.
68. Gao, F.; Teplyakov, A. V., Reaction of Hydrazine with a Chlorine-Terminated Si(111) Surface. *J. Phys. Chem. C* **2014,** 118, 27998-28006.
69. Huey, W. L. B.; Goldberger, J. E., Covalent functionalization of two-dimensional group 14 graphane analogues. *Chem. Soc. Rev.* **2018,** 47, 6201-6223.
70. Harris, R. K.; Becker, E. D.; Cabral de Menezes, S. M.; Goodfellow, R.; Granger, P., NMR Nomenclature: Nuclear Spin Properties and Conventions for Chemical Shifts: IUPAC Recommendations 2001. *Solid State Nucl. Magn. Reson.* **2002,** 22, (4), 458-483.
71. Hung, I.; Gor'kov, P.; Gan, Z., Using the heteronuclear Bloch-Siegert shift of protons for B1 calibration of insensitive nuclei not present in the sample. *J. Magn. Reson.* **2020,** 310, 106636.
72. Sakellariou, D.; Lesage, A.; Hodgkinson, P.; Emsley, L., Homonuclear dipolar decoupling in solid-state NMR using continuous phase modulation. *Chem. Phys. Lett.* **2000,** 319, 253-260.
73. Meiboom, S.; Gill, D., Modified Spin-Echo Method for Measuring Nuclear Relaxation Times. *Rev. Sci. Instr.* **1958,** 29, 688-691.
74. Fung, B. M.; Khitrin, A. K.; Ermolaev, K., An Improved Broadband Decoupling Sequence for Liquid Crystals and Solids. *J. Magn. Reson.* **2000,** 142, 97-101.
75. Bak, M.; Rasmussen, J. T.; Nielsen, N. C., SIMPSON: A General Simulation Program for Solid-State NMR Spectroscopy. *J. Magn. Reson.* **2000,** 147, 296-330.
76. Tošner, Z.; Vosegaard, T.; Kehlet, C.; Khaneja, N.; Glaser, S. J.; Nielsen, N. C., Optimal Control in NMR Spectroscopy: Numerical Implementation in SIMPSON. *J. Magn. Reson.* **2009,** 197, 120-134.
77. Tošner, Z.; Andersen, R.; Stevensson, B.; Edén, M.; Nielsen, N. C.; Vosegaard, T., Computer-Intensive Simulation of Solid-State NMR Experiments using SIMPSON. *J. Magn. Reson.* **2014,** 246, 79-93.
78. Clark, S. J.; Segall, M. D.; Pickard, C. J.; Hasnip, P. J.; Probert, M. I. J.; Refson, K.; Payne, M. C., First Principles Methods using CASTEP. *Z. Kristallogr. - Cryst. Mater.* **2005,** 220, 567-570.
79. Perdew, J. P.; Burke, K.; Ernzerhof, M., Generalized Gradient Approximation Made Simple. *Phys. Rev. Lett.* **1996,** 77, 3865-3868.
80. Tkatchenko, A.; Scheffler, M., Accurate Molecular Van Der Waals Interactions from Ground-State Electron Density and Free-Atom Reference Data. *Phys. Rev. Lett.* **2009,** 102, 073005.
81. Vanderbilt, D., Soft Self-Consistent Pseudopotentials in a Generalized Eigenvalue Formalism. *Phys. Rev. B* **1990,** 41, 7892-7895.
82. Green, T. F. G.; Yates, J. R., Relativistic Nuclear Magnetic Resonance J-coupling with Ultrasoft Pseudopotentials and the Zeroth-Order Regular Approximation. *J. Chem. Phys.* **2014,** 140, 234106.

Table of Contents Graphic